The middle Eocene climatic optimum event in the Contessa Highway section, Umbrian Apennines, Italy

Luigi Jovane
Istituto Nazionale di Geofisica e Vulcanologia, Via di Vigna Murata 605, 00143 Rome, Italy, and *Dipartimento di Fisica, Università di Bologna, Via Berti Pichat 8, 40127, Bologna, Italy*

Fabio Florindo[†]
Istituto Nazionale di Geofisica e Vulcanologia, Via di Vigna Murata 605, 00143 Rome, Italy

Rodolfo Coccioni
Istituto di Geologia e Centro di Geobiologia, Università degli Studi di Urbino "Carlo Bo," Campus Scientifico, Località Crocicchia, 61029 Urbino, Italy

Jaume Dinarès-Turell
Istituto Nazionale di Geofisica e Vulcanologia, Via di Vigna Murata 605, 00143 Rome, Italy

Andrea Marsili
Istituto di Geologia e Centro di Geobiologia, Università degli Studi di Urbino "Carlo Bo," Campus Scientifico, Località Crocicchia, 61029 Urbino, Italy

Simonetta Monechi
Dipartimento di Scienze della Terra, Università degli Studi di Firenze, Via La Pira 4, 50121 Florence, Italy

Andrew P. Roberts
National Oceanography Centre, University of Southampton, European Way, Southampton SO14 3ZH, UK

Mario Sprovieri
Istituto Ambiente Marino Costiero, Consiglio Nazionale delle Ricerche (CNR), Calata Porta di Massa (Interno Porto di Napoli), 80133 Naples, Italy

ABSTRACT

We report a high-resolution paleomagnetic investigation constrained by new qualitative and semiquantitative analyses of planktic and benthic foraminifera, nannofossil assemblages, integrated with oxygen and carbon isotope measurements, for the middle Eocene Scaglia limestones of the Contessa Highway section, central Italy. Calcareous plankton assemblages enable recognition of several biostratigraphic events from planktic foraminiferal zone P11 to the lower part of zone P15 and from calcareous nannofossil zone NP15 to the upper part of zone NP17, which results in refinement of the magnetobiostratigraphy of the Contessa Highway section. Correlation of the paleomagnetic polarity pattern with the geomagnetic polarity time scale provides a direct age interpretation for strata around the middle Eocene Scaglia limestones of the Contessa Highway section, from chrons C21n (47 Ma) through to subchron C18n.1n (38.5 Ma). Bulk carbon isotope values indicate a distinct carbon isotopic shift at 40 Ma that is interpreted to represent the first evidence in the Northern Hemisphere of the middle Eocene climatic optimum, which has recently been observed as a stable isotope anomaly in multiple records from the Indian-Atlantic sector of the Southern Ocean. This demonstrates a global response of the carbon cycle to the proposed transient increased pCO_2 levels during the late middle Eocene and consequent global CO_2-driven climate change.

Keywords: Eocene, middle Eocene climatic optimum, MECO, magnetostratigraphy, biostratigraphy, stable isotope stratigraphy, Contessa Highway section, Italy.

INTRODUCTION

Deep-sea stable isotope records indicate a general high-latitude cooling trend over the past 50 m.y. (from the early Eocene climatic optimum or EECO), which is thought to have resulted from a combination of factors that altered the amount and distribution of solar radiation over Earth's surface (e.g., Shackleton and Kennett, 1975; Miller et al., 1991; Zachos et al., 2001; Lear et al., 2004). The ~4‰ increasing trend in $\delta^{18}O$ is not monotonic. It is complex and is composed of a series of significant short-term cooling and warming phases, ranging in temporal extent from 10^3 to 10^5 yr (e.g., the Oi-1 event in the earliest Oligocene at 34 Ma and the Mi-1 event in the earliest Miocene at 23 Ma; Miller et al., 1991). These signals are superimposed on a long-term trend toward progressively cooler conditions since 50 Ma.

Recently, a distinct negative shift in $\delta^{18}O$ values at 41.5 Ma (designated as the middle

[†]Corresponding author e-mail: florindo@ingv.it.

GSA Bulletin; March/April 2007; v. 119; no. 3/4; p. 413–427; doi: 10.1130/B25917.1; 10 figures.

Eocene climatic optimum) has been observed in cores from the Indian and Atlantic sectors of the Southern Ocean, and it has been interpreted primarily as a temperature signal that affected both surface waters and middle bathyal deep waters (Bohaty and Zachos, 2003). This peak warming is not mirrored by a significant negative $\delta^{13}C$ excursion, as observed during the Paleocene-Eocene thermal maximum, which suggests that the middle Eocene climatic optimum event was not triggered by methane-hydrate dissociation but by a transient rise in pCO_2 levels.

The middle Eocene time interval is well represented in pelagic carbonates of the Italian Scaglia Rossa and Scaglia Variegata Formations. The Contessa sections (Gubbio, central Italy) contain a thick and continuous Scaglia sequence that extends from the Lower Cretaceous through to the Upper Miocene (e.g., Lowrie et al., 1982; Cresta et al., 1989; Montanari et al., 1997). The Middle and Upper Eocene Scaglia limestones that crop out along the Contessa Highway (CH) section have been paleomagnetically investigated by Lowrie et al. (1982). In the same stratigraphic interval that we describe in this paper, Lowrie et al. (1982) collected samples with an average stratigraphic spacing of ~80 cm. They stated that: "the chosen sample spacing was too wide to describe the shorter magnetozones completely" (see also Figure 3 of Lowrie et al., 1982). A higher-resolution paleomagnetic reinvestigation was implicitly suggested by this statement. In order to: (1) improve the magnetostratigraphic resolution of the late middle Eocene interval, (2) provide a calibration of biostratigraphic datums in the same interval, and (3) test whether a signature associated with the middle Eocene climatic optimum event is present in this Northern Hemisphere sequence, which might suggest a global extent for the middle Eocene climatic optimum event, we have developed a new magnetobiostratigraphy, which we integrate with new oxygen and carbon isotope measurements, for the middle Eocene Scaglia limestones of the Contessa Highway section.

LOCATION AND GEOLOGICAL SETTING

The Contessa Highway section (lat. 43°22′47″N; long. 13°33′49″E) is located in the Umbrian region (northeastern Apennines), a few kilometers northwest of Gubbio, which is one of the most ancient towns of Umbria (Fig. 1). In this region, depositional environments evolved from a Triassic-Liassic carbonate-shelf setting on the continental margin of an African plate promontory, or "Adria" (Channell et al., 1979), located on the southern margin of the Tethys Ocean, to a pelagic setting (lower to upper bathyal environments), which extended into the Paleogene. The investigated section is fresh and is continuously exposed along a road cut (along Highway 452, the Contessa Road). It is ~200 m thick and extends from the Cretaceous-Tertiary (K-T) boundary through to the Upper Oligocene and consists of the upper part of the Scaglia Rossa (early Turonian to middle Eocene), the Scaglia Variegata (middle Eocene to late Eocene), and the Scaglia Cinerea (late Eocene to Oligocene) (e.g., Cresta et al., 1989). The Paleogene portion of the Scaglia Rossa is made up of 82 m of well-stratified red to pinkish limestones and marly limestones. From 50 to 88 m above the K-T boundary, chert nodules are associated with the limestones ("upper cherty member" of Lowrie et al., 1982). During the middle Eocene, the amount of clay increased, and the Scaglia Rossa grades into ~80 m of gray, green, and red bedded marly limestones and calcareous marls of the Scaglia Variegata Formation, which are the focus of this study. The boundary between the Scaglia Rossa and the Scaglia Variegata Formations is conventionally placed at 88 m above the K-T boundary, which coincides with the uppermost cherty limestone horizon. In agreement with Monaco et al. (1987), the top of the Scaglia Variegata (upper late Eocene; not studied here) is conventionally placed at the "upper reddish interval," which marks the passage to the overlying Scaglia Cinerea marls. This formation is characterized by alternating gray marly limestones and gray marls that were deposited throughout the Oligocene.

The Scaglia Variegata Formation has clear cyclicity within the Contessa Highway section, with bundles of limestone-marl couplets that suggest the possibility of orbitally controlled deposition (Fig. 2). We identified the clear white marker bed at ~99 m, and, from ~110 to 140 m, the distinctive marker beds (clay horizons) are termed K, L, M, N, O, P, and Q, as described by Lowrie et al. (1982). The bedding dips 60° to 72° toward the northeast (azimuth of 40° to 54°). A major fault, not described before, occurs in the upper part of the Scaglia Variegata from 139.50 to 140 m, a few meters above the Q recessed interval. The fault dips north at 40° and is connected to two splays that dip south at 70°. The fault planes present both dip-slip and strike-slip slickensides.

Previous Paleomagnetic Investigation of the Contessa Highway

In the previous paleomagnetic investigation of the middle and upper Eocene Scaglia limestones of the Contessa Highway section (Lowrie et al., 1982), the same stratigraphic interval was studied (i.e., from 90 to 150 m above the K-T boundary), and samples were collected at an average spacing of ~80 cm. The remanent magnetizations were measured with a 3-axis ScT cryogenic magnetometer (Goree and Fuller, 1976). Pilot samples, selected at ~4 m intervals, were used to assess the most suitable demagnetization technique for routine treatment. Based on the demagnetization behavior of the pilot samples, Lowrie et al. (1982) found that thermal treatment was more effective than stepwise alternating field (AF) demagnetization in isolating the characteristic remanent magnetization (ChRM) component in the Scaglia lithologies. The ChRM was generally well defined above 300 °C in the Variegata and above 400 °C in the Scaglia Rossa samples. It is noteworthy that a small component of magnetization consistently persisted above 600 °C. The magnetic reversal stratigraphy for the interval from 95 to 150 m, integrated with planktic foraminiferal biostratigraphy, was correlated with the geomagnetic reversal sequence corresponding to oceanic magnetic anomalies 17–21 (LaBrecque et al., 1977). A rock magnetic investigation was also carried out, and, based on coercivity spectrum analysis, Lowrie et al. (1982) provided evidence that the main magnetic mineral is magnetite, and a hematite component is pronounced in dark-reddish Paleocene Scaglia samples (not studied here).

METHODS

Before sampling, and in order to evaluate possible orbital forcing in the studied strata (in progress), a bed-by-bed lithological log was constructed during several field trips (Fig. 2).

Paleomagnetism—Sampling

The sampled interval of the Scaglia Variegata Formation extends from 95 to 150 m above the base of the section. We collected 192 oriented block samples at 5–30 cm intervals and located them with respect to the black and white markers painted onto the section at 5 m stratigraphic intervals by Lowrie et al. (1982). The sample spacing was designed to be closer at reversal boundaries to enable identification of reversals at the individual bed level. Higher-resolution sampling was hampered by the presence of a metallic net that is used to maintain slope stability of the road cut. Each oriented hand sample was cut in the laboratory and generally yielded two or more 10 cm^3 samples.

Paleomagnetism—Laboratory Procedures and Analysis

Paleomagnetic analyses were carried out within a magnetically shielded laboratory at the

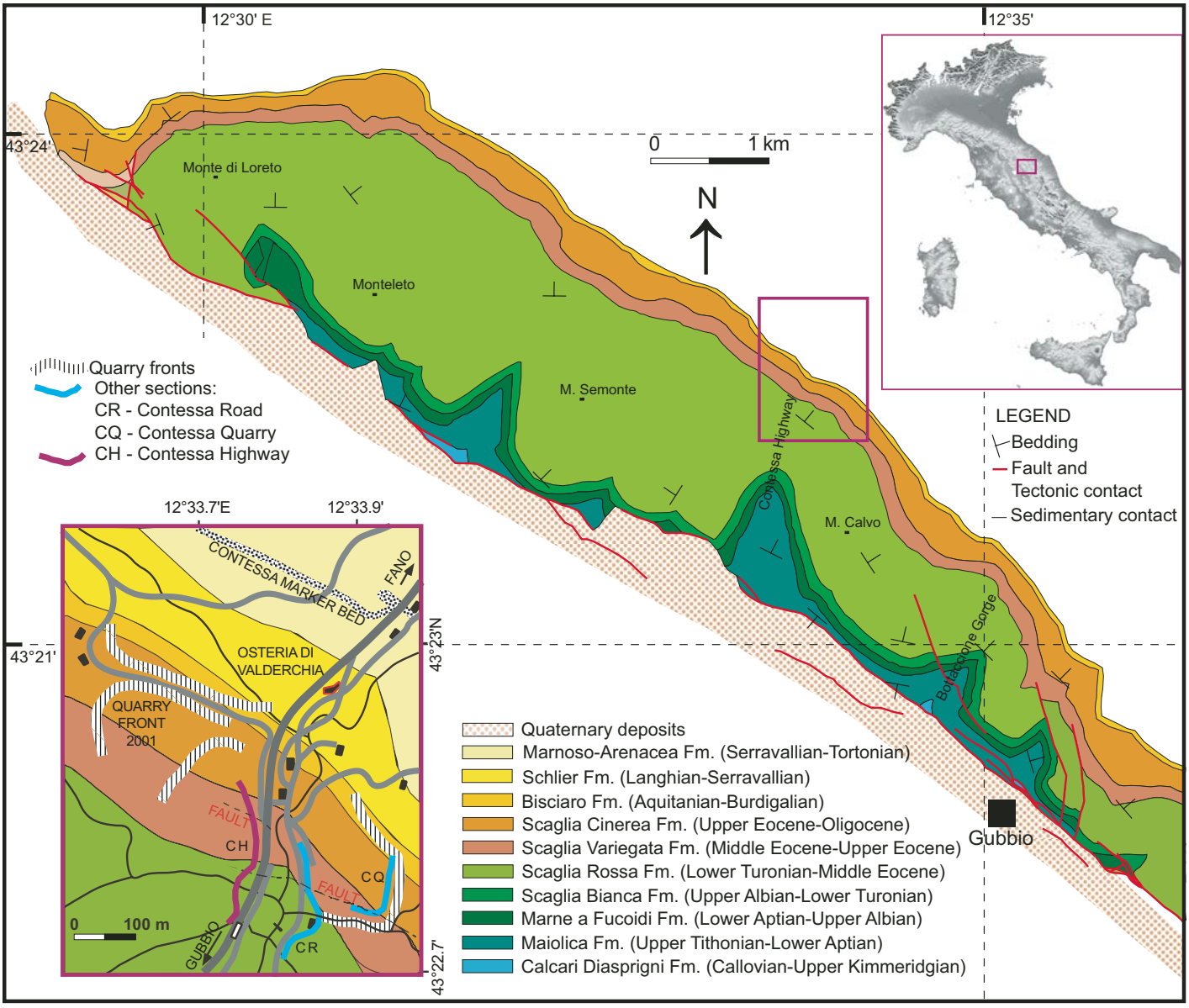

Figure 1. Schematic geological map of the NW-SE–trending Gubbio structure and location of the Contessa sections (CH—Contessa Highway; CQ—Contessa Quarry; CR—Contessa Road) on a simplified map that gives the formation boundaries in the Contessa Valley.

Istituto Nazionale di Geofisica e Vulcanologia (INGV), Rome. Natural and artificial magnetic remanences were measured using a narrow-access pass-through cryogenic magnetometer (2-G Enterprises model 750R) with in-line AF demagnetization capability. One sample from each stratigraphic level was AF demagnetized at successive peak fields of 5, 10, 15, 20, 25, 30, 40, 50, 60, 80, and 100 millitesla (mT). Next, sister samples were thermally demagnetized using a magnetically shielded Pyrex furnace at 100, 200, 300, 330, 360, 400, 450, 500, 550, 600, 650, and 700 °C. The low-field magnetic susceptibility (χ) was measured after each heating step to monitor for thermal alteration of the magnetic minerals. Thermal and AF demagnetization data were examined using orthogonal vector component diagrams (Zijderveld, 1967); best-fit lines for the progressive demagnetization data were evaluated by principal component analysis (Kirschvink, 1980).

A range of rock magnetic measurements was used to investigate the magnetic mineralogy throughout the investigated section. The low-field mass-specific magnetic susceptibility (χ) was measured with a Kappabridge KLY-2 magnetic susceptibility meter. Artificial remanences were also measured, including the anhysteretic remanent magnetization (ARM) imparted in a 100 mT AF, with a superimposed 0.05 mT DC bias field, the isothermal remanent magnetization (IRM) imparted in a field of 0.9 T, and back-field demagnetization of the IRM at 0.1 T and 0.3 T. These data were used to determine the S-ratio ($IRM_{-0.3\ T}/IRM_{0.9\ T}$) and the HIRM (HIRM = $[IRM_{0.9\ T} + IRM_{-0.3\ T}]/2$). These remanences were measured with the 2-G Enterprises magnetometer. The temperature dependence of magnetic susceptibility was measured up to 700 °C on selected samples using a furnace-equipped Kappabridge KLY-3 magnetic susceptibility meter. First-order reversal curves (FORCs) were analyzed on sediment chip samples, using a Princeton Measurements Corporation MicroMag vibrating sample magnetometer

Figure 2. Detailed lithostratigraphic column for the interval between 95 and 151 m for the Contessa Highway section. Samples collected for this study and colors of the lithologies are also indicated. The white marker bed and the distinctive marker beds (clay horizons) are termed K, L, M, N, O, P, and Q, as described by Lowrie et al. (1982).

at the National Oceanography Centre Southampton (NOCS), University of Southampton, UK. Samples were selected for FORC analysis (Roberts et al., 2000) from the intervals with strongest magnetizations.

Foraminiferal Assemblages

One hundred and sixty samples were collected (at 30 cm average intervals) for biostratigraphic and stable isotope analyses. The foraminiferal content was analyzed for all samples. Foraminifera were studied in washed residues from soft and hard lithologies. Preparation from soft lithologies included gentle crushing, soaking in a hydrogen peroxide solution (10%), sieving through a 63 μm mesh, and drying at 60 °C. Preparation from hard lithologies included gentle crushing, cold acetolysis with acetic acid (80%) following the method of Lirer (2000), sieving through a 63 μm mesh, 1 to 2 h cleaning in an ultrasonic cleaner, and drying at 60 °C. The cold acetolysis method enabled extraction of generally easily identifiable foraminifera even from indurated limestones. This offered the possibility of accurate taxonomic determination and detailed analysis of foraminiferal assemblages.

Nannofossil Assemblages

Samples for calcareous nannofossil analysis were prepared as smear slides using standard techniques (Bown and Young, 1998). Nannofossils were examined with a light microscope at a magnification of 1000× and were identified following the taxonomic schemes of Perch-Nielsen (1985) and Varol (1998). Assemblages were studied semiquantitatively, and at least three traverses were investigated for each smear-slide.

Oxygen and Carbon Isotope Measurements

One hundred thirty-four stable isotope analyses were made on bulk samples. They were made using an automated continuous-flow carbonate preparation GasBenchII device (Spötl and Vennemann, 2003) and a ThermoElectron Delta Plus XP mass spectrometer at the Istituto Ambiente Marino Costiero, Consiglio Nazionale delle Ricerche (IAMC-CNR, Naples) isotope geochemistry laboratory. Acidification of samples was performed at 50 °C. An internal standard (Carrara Marble with $\delta^{18}O = -2.43$ versus Vienna Peedee belemnite [VPDB] and $\delta^{13}C = 2.43$ versus VPDB) was run for every 6 samples, and, for every 30 samples, the NBS19 international standard was measured. Standard deviations of carbon and oxygen isotope measurements were estimated at 0.1‰ and 0.08‰, respectively, on the basis of replicate measurements of ~70 samples. The entire calibration was based directly on standard materials that were part of each run (in our case, the homogeneous and certified Carrara Marble carbonate with isotopic composition determined by conventional offline dual-inlet techniques), rather than from solving fractionation equations for the acid-based reaction. In other words, there was no need to know the stable isotopic composition of the CO_2 reference gas a priori, nor the acid fractionation factor at the given temperature of the reaction (Spötl and Vennemann, 2003). All of the stable isotope data are reported in per mil (‰) relative to the VPDB standard.

RESULTS

Paleomagnetic Behavior and Polarity Zonation

NRM intensities were generally low (Fig. 3), especially in the uppermost 10 m of the studied interval (i.e., above 140 m), although there were significant fluctuations (NRM ranges from 6.6×10^{-9} Am^2/kg to 1.1×10^{-5} Am^2/kg; mean = 2.4×10^{-7} Am^2/kg). Intervals with weak magnetizations had more complex behavior during demagnetization (Fig. 4). Based on the observed demagnetization behavior, thermal treatment was more effective than stepwise AF demagnetization in removing secondary components and in isolating the ChRM component for both normal and reversed polarity samples (see also Lowrie et al., 1982). Stable paleomagnetic behavior was evident from 92% of the thermally demagnetized samples and from 58% of the AF demagnetized samples. In particular, AF treatment was not effective in removing secondary magnetization components from red-colored intervals.

The magnetic polarity record of the studied portion of the Contessa Highway section can be subdivided into seven magnetozones, where the magnetozones are defined as intervals with multiple, consecutive samples with polarities that are distinctly different from neighboring intervals (Fig. 5). In a few cases (e.g., 96.90 m, 103.30 m, and 133.95 m), isolated samples have polarities opposite to those of the rest of the magnetozone. These samples are not considered in the overall polarity zonation.

Starting from the bottom, the lower 1.08 m of the magnetic polarity record has three samples with stable normal polarity (magnetozone N1); the lower boundary of this magnetozone was not sampled. Above magnetozone N1, a predominantly reversed polarity magnetozone dominates from 96.08 m to 110.39 m (magnetozone R1). There is a normal polarity interval from 110.39 to 119.80 m (magnetozone N2), which is followed by a well-defined reversed polarity interval (magnetozone R2) from 119.80 to 127.45 m. Magnetozone R2 is separated from the overlying reversed polarity interval R3 (from 128.63 to 135.29 m) by a thin (1.21-m-thick), but clearly defined, normal polarity interval (N3) that extends from 127.45 to 128.63 m. The uppermost 12.71 m of the studied sequence is dominated by normal polarity (>135.29 m; magnetozone N4). In this magnetozone, two samples (at 140.45 and 140.60 m) have reverse polarity. The presence of the aforementioned fault zone contributes to interpretational difficulties in this thin interval (see following).

Rock Magnetic Properties

Demagnetization behavior, coercivity parameters (S-ratio, HIRM), FORC diagrams, and thermomagnetic analyses all indicate that the magnetic mineral assemblage is dominated by a complex mixture of magnetic minerals that includes magnetite (dominant), maghemite, and hematite (Figs. 6–8). Among these, the presence of magnetite is indicated in some intervals by S-ratios with values close to unity (Fig. 6), marked thermal unblocking at 580 °C (Fig. 7), and a peak near the origin of the FORC diagram (Fig. 8). On the other hand, the presence of hematite is indicated by low S-ratios, high values of HIRM (Fig. 6), marked thermal unblocking at 680 °C (Fig. 7), and a small peak of the FORC distribution at high coercivities of >200–250 mT (Fig. 8). Marked decreases in susceptibility were observed after heating to 250–300 °C during thermal demagnetization, especially in the reddish intervals (e.g., Fig. 7C), which we attribute to the presence of maghemite (thermally induced conversion from maghemite to hematite; Stacey and Banerjee, 1974). The abrupt increase in magnetic susceptibility above 400–450 °C for most samples (Fig. 4) is attributed to thermally induced growth of new magnetite due to the breakdown of smectite during thermal demagnetization (smectite is the dominant clay mineral in the Scaglia Variegata Formation; Guerrera et al., 1988; Mattias et al., 1989).

Interpretation of standard magnetic parameters is complicated in the presence of variable mixtures of magnetic minerals. Regardless, some clear patterns are evident. Only above 140.5 m and at 126–127 m and 116.50–120 m is magnetite the dominant magnetic mineral, without evidence of relatively high coercivity minerals such as hematite (indicated by S-ratios in Fig. 6). On the other hand, as would be expected, the stratigraphic intervals with stronger red colorations (95–111 m and 135–139 m) contain significant concentrations of hematite, as indicated by higher HIRM values and lower S-ratios (Fig. 6). It should be noted that the boundary between

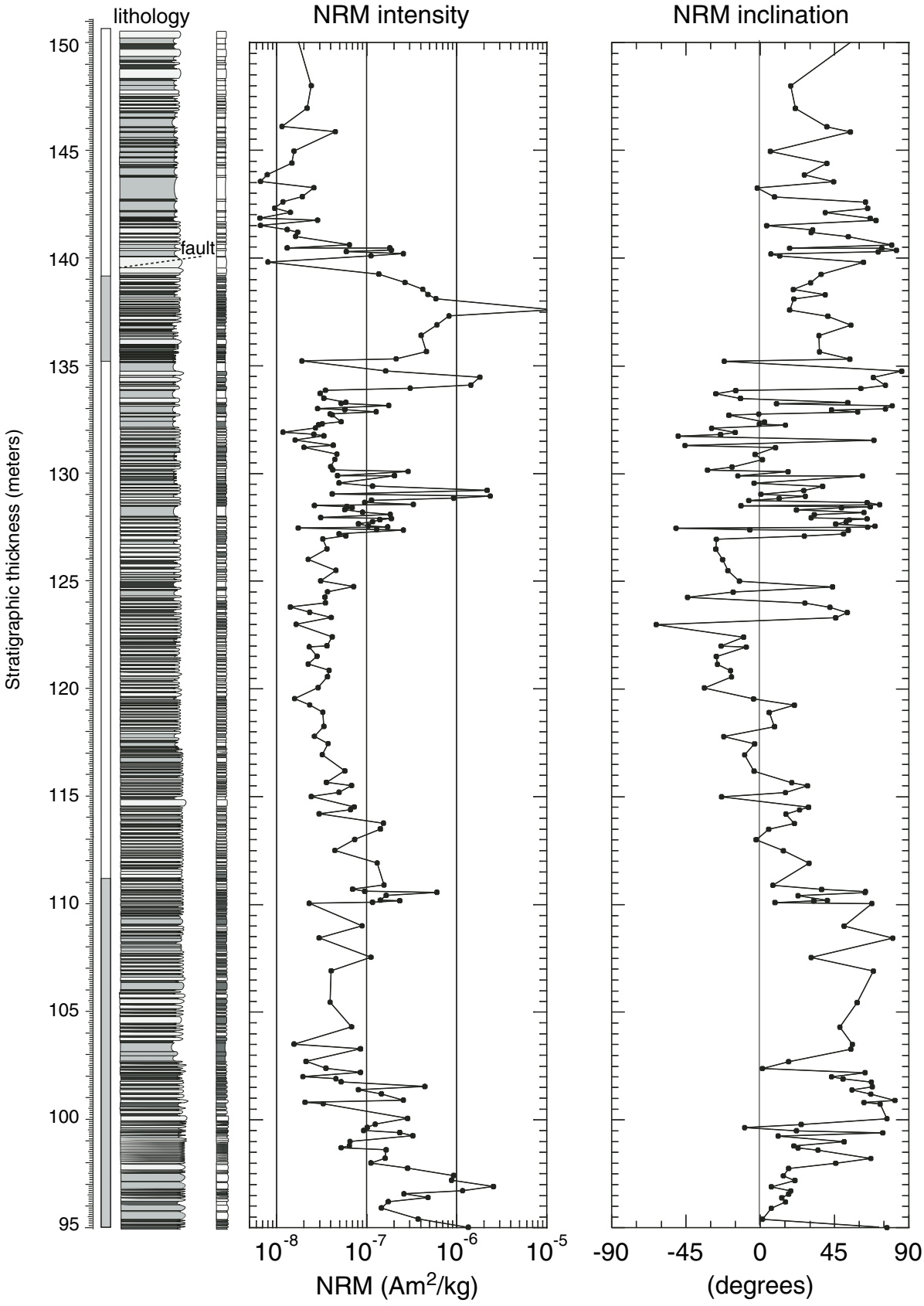

Figure 3. Stratigraphic variations of intensity and inclination of the natural remanent magnetization (NRM). A detailed lithostratigraphic column for the interval between 95 and 151 m is shown to the left.

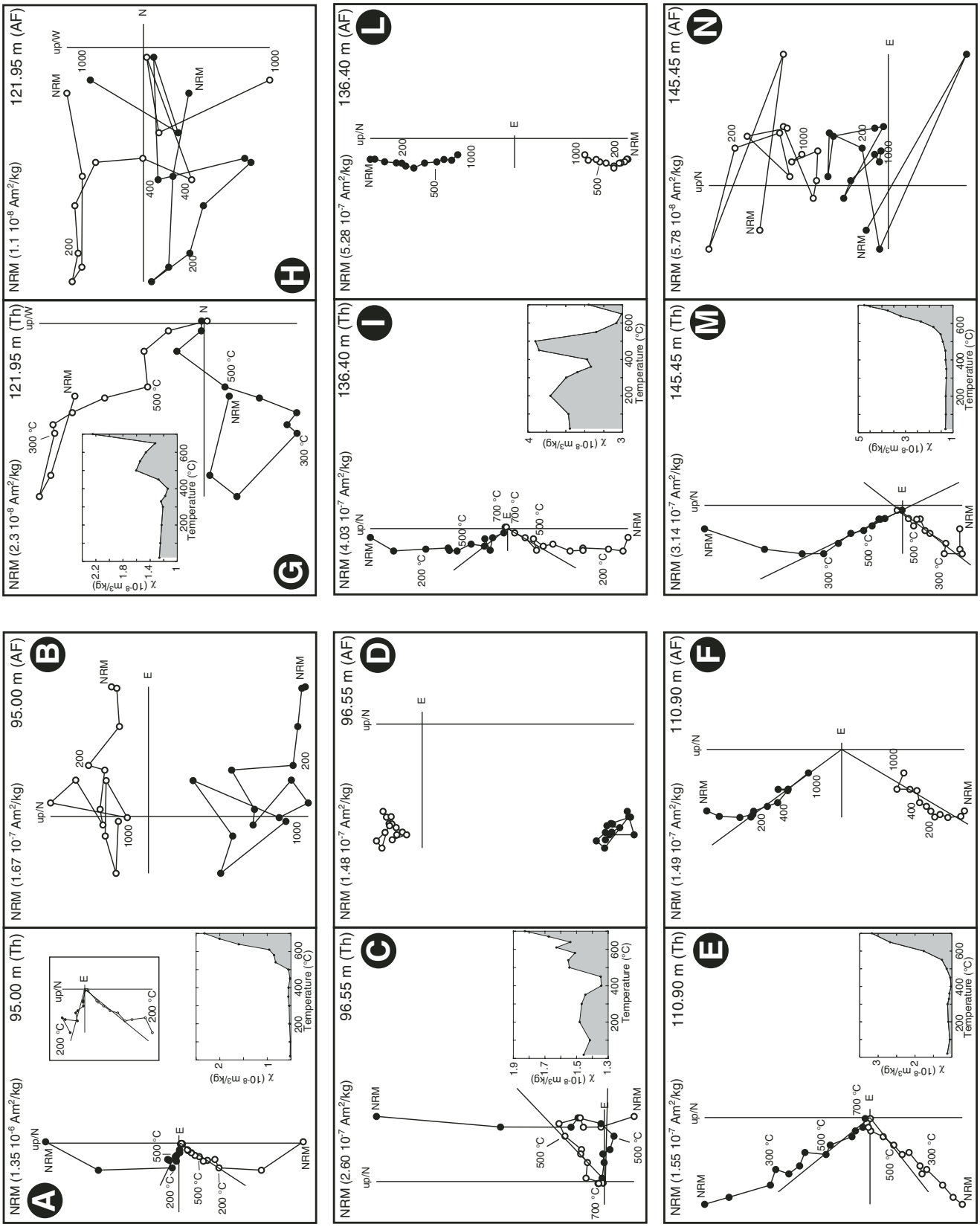

Figure 4. Thermal and alternating field (AF) demagnetization diagrams in tilt-corrected coordinates for six representative "sister" specimens. Open circles—projection onto the vertical plane; full circles—projection onto the horizontal plane. Best-fit lines are only shown for samples with identifiable characteristic remanent magnetization (ChRM) components. NRM—natural remanent magnetization. Insets: Magnetic susceptibility measurements made after each heating step for thermal demagnetization.

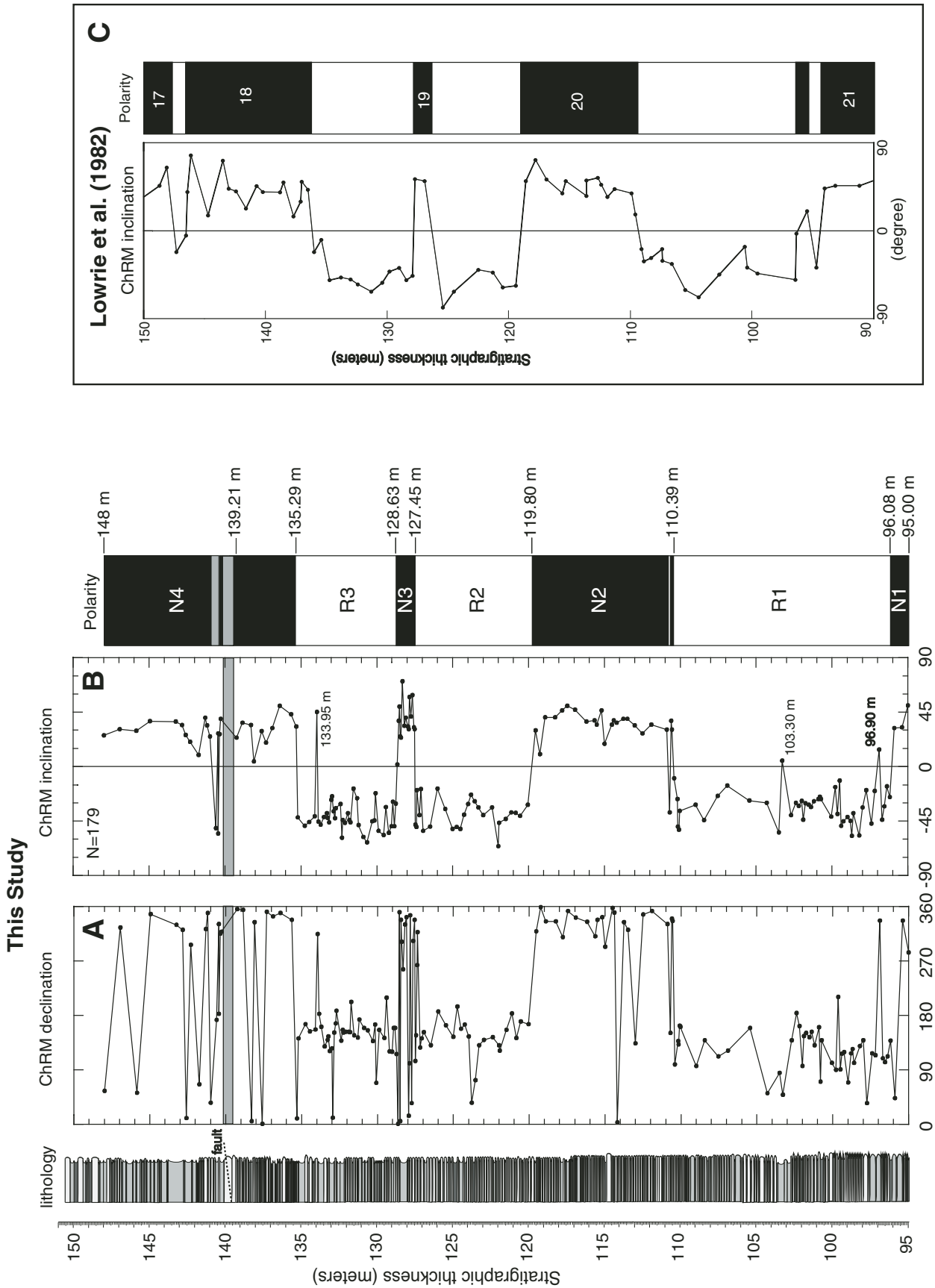

Figure 5. Stratigraphic variations of (A) declination and (B) inclination of the characteristic remanent magnetization (ChRM). The magnetic polarity zonation is shown on the log to the right. Black (white) represents normal (reversed) polarity intervals. A few isolated samples have polarities opposite to those of the rest of the magnetozone (e.g., 96.90 m, 103.30 m, and 133.95 m), and these are not considered in the overall polarity zonation. (C) Inclination variations of the ChRM for the same sequence from Lowrie et al. (1982).

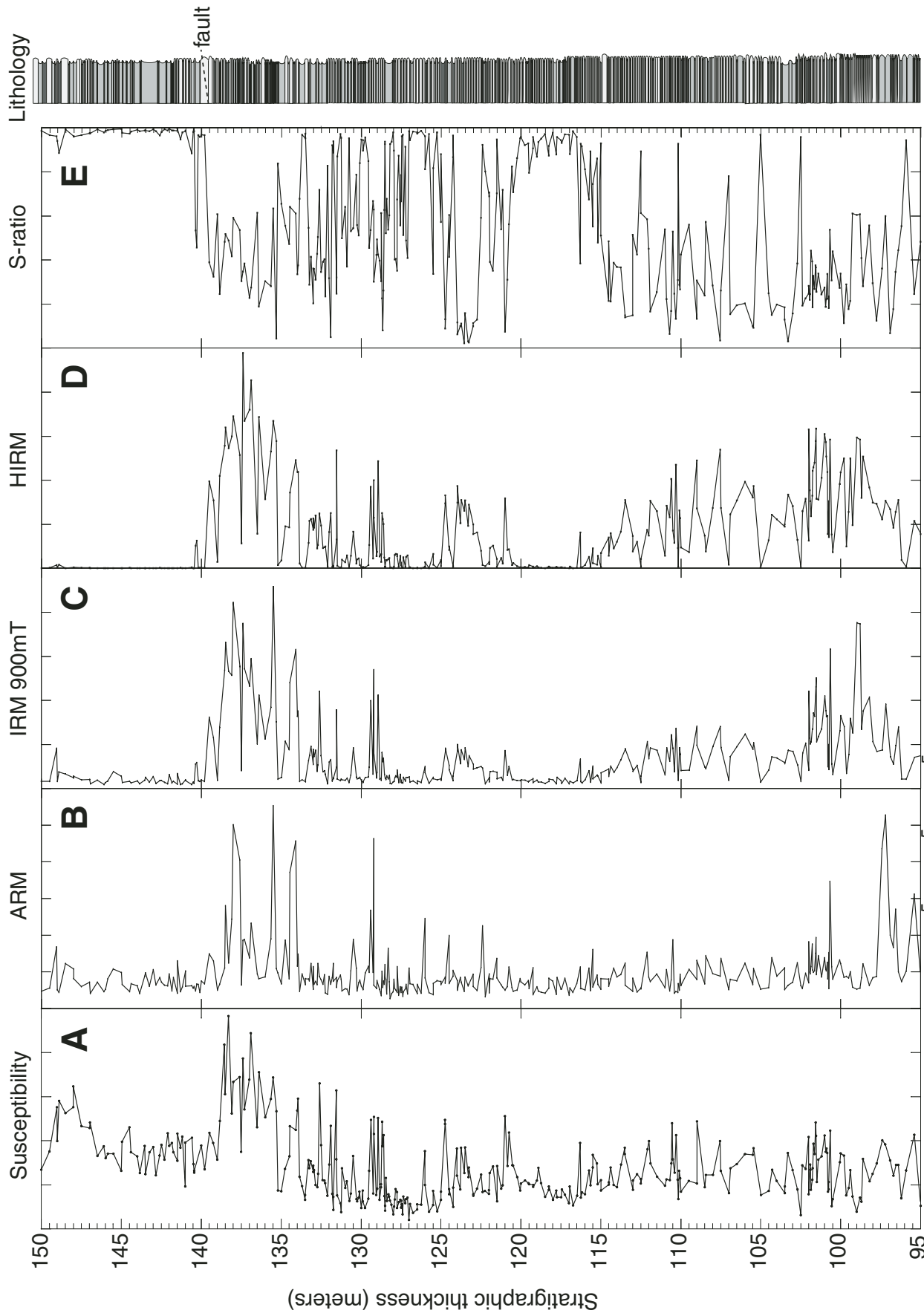

Figure 6. Stratigraphic variations in magnetic properties for the Contessa Highway section, including low-field magnetic susceptibility, anhysteretic remanent magnetization (ARM), isothermal remanent magnetization (IRM), HIRM (= [$IRM_{0.9\,T}$ + $IRM_{-0.3\,T}$]/2), S-ratio (= $IRM_{-0.3\,T}$/$IRM_{0.9\,T}$). A detailed lithostratigraphic column for the interval between 95 and 151 m is shown to the right. See text for discussion.

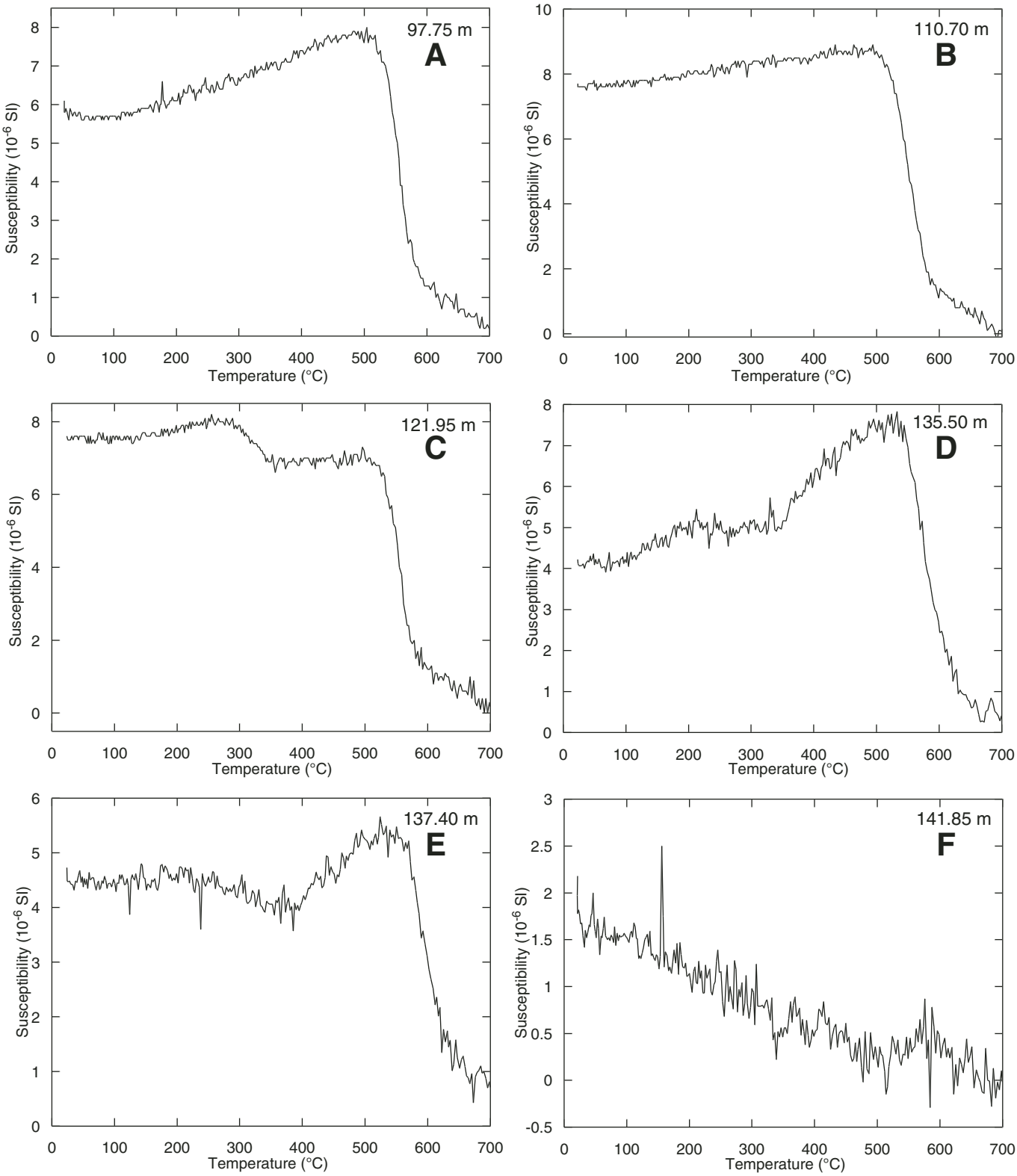

Figure 7. Temperature dependence of magnetic susceptibility for six selected samples up to a maximum temperature of 700 °C. A clear decrease in susceptibility is evident near 580 °C for most of these samples, which indicates the Curie temperature of magnetite. Moreover, some samples (e.g., 121.95 m) also display a broad bump centered at 250 °C followed by a marked decrease in magnetic susceptibility, which can be interpreted in terms of conversion from maghemite to hematite (e.g., Stacey and Banerjee, 1974). Above 600 °C, the magnetic susceptibility is weak compared to the sensitivity of the instrument, but it is still possible to discern evidence of the Néel temperature of hematite (680 °C). The data are corrected for the diamagnetism of the furnace.

the uppermost magnetite-dominated interval and the thick underlying interval, with a complex mixture of magnetic minerals, corresponds to the fault zone at 139.5–140 m (Fig. 6). This evidence suggests that a portion of the record could be missing at the fault.

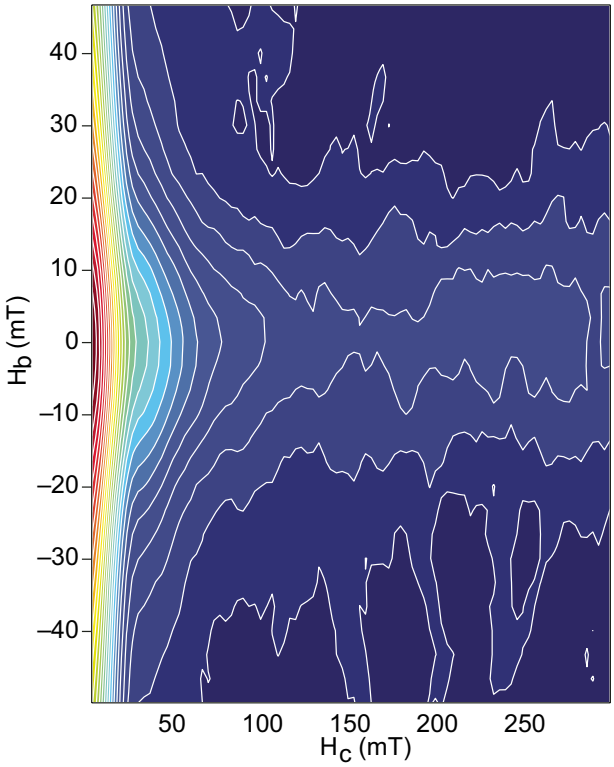

Figure 8. Representative first-order reversal curve (FORC) diagram (smoothing factor [SF] = 9) for a sample from 131.40 m. The dominant peak near the origin is consistent with the presence of magnetite, while the small peak at H_c = 200–250 mT indicates the presence of a high-coercivity mineral (e.g., hematite).

Foraminiferal Assemblages

Foraminifera are continuously present, abundant, and diverse throughout the studied section. Preservation varies from poor to good, but is mostly moderate. Paleocene to Lower Eocene specimens are occasionally present. The Contessa Highway section has been previously correlated to the Paleogene planktonic foraminiferal zonation by Lowrie et al. (1982), following the zonal schemes of Bolli (1957a, 1957b, 1966), Blow (1969, 1979), and Premoli Silva and Bolli (1973). Additional biostratigraphic data are also given by Verducci and Nocchi (2004) following Premoli Silva et al. (2003) and are in agreement with the criteria used by Pearson and Chaisson (1997).

All of the marker species that define the standard planktonic foraminiferal zones of Berggren et al. (1995) through most of the middle Eocene occur in the analyzed material. The lower part of the studied section contains *Morozovella aragonensis* and belongs to the P11 zone (*Globigerapsis kugleri*/*Morozovella aragonensis* concurrent range zone). The last occurrence (LO) of this species, which defines the P11/P12 (*Morozovella lehneri* partial range zone) zonal boundary, occurs at 112.50 m (Fig. 9). The first occurrence (FO) and the LO of *Orbulinoides beckmanni,* which mark, respectively, the P12/P13 (*Globigerapsis beckmanni* total range zone) and the P13/P14 (*Truncorotaloides rohri–Morozovella spinulosa* partial range zone) zonal boundaries, are documented at 135 m and 137 m, respectively (Fig. 9).

The LO of large acarinids occurs at 144 m (Fig. 9). The LO of *Morozovella spinulosa,* which is the last representative of the *Morozovella* genus, is recognizable at 146 m, where *Truncorotaloides rohri* also disappears. The FO of *Globigerinatheka semiinvoluta* is recorded at 148 m and defines the P14/P15 (*Porticulasphaera semiinvoluta* interval zone) zone boundary.

Paleobathymetric assessment is based on the distribution of index forms as reported by Van Morkhoven et al. (1986). The lack of faunal components typical of abyssal depths provides a lower depth limit of 2000 m. The high abundance of *Cibicidoides eocaenus*, *C. mexicanus*, *Globocassidulina subglobosa*, *Hanzawaia ammophila*, *Nuttallides truempyi*, and *Planulina costata,* together with some specimens of *Aragonia aragonensis,* indicates a middle-lower bathyal setting (800–1000 m). Although some of the bathymetric indicators fluctuate in relative abundance or even locally disappear, no remarkable paleobathymetric change is evident throughout the studied section. Accordingly, the P/(P+B) × 100 (%) (P = planktic; B = benthic) ratio has constant values that are typical of bathyal depositional environments.

Nannofossil Assemblages

Calcareous nannofossils are abundant throughout the studied interval, even if they are not well preserved and have low diversity. Most of the important markers used to define the standard zonations of Martini (1971) and Okada and Bukry (1980) occur. Several additional marker species are also documented here.

Monechi and Thierstein (1985) reported biostratigraphic results from the Eocene interval of the Contessa Highway section using the Paleogene coccolith (CP) zones of Okada and Bukry (1980). Our re-examination of the interval allows recognition of several important and well-known markers, such as the FO and LO of *Chiasmolithus gigas* (CP13b subzone). *Chiasmolithus* is not common in the Scaglia Formation owing to paleoecological and preservation problems; low relative abundances have led to discontinuous occurrences. Regardless, FO and LO determinations are moderately reliable. While a few specimens of *Reticulofenestra umbilica* >14 µm are present above 119 m, we define its first common occurrence (FCO) at 122 m, together with the LO of *Nannotetrina* spp. (Fig. 9). A discrepancy between this identification and that of Monechi and Thierstein (1985) is due to the different taxonomic concept of *R. umbilica* size >12.5 µm in Monechi and Thierstein (1985).

Several additional calcareous nannofossil events can be used to improve the biostratigraphic framework. The FO and LO of *Sphenolithus furcatolithoides*, two events reported by Catanzariti and Perilli (2004) in Eocene Formations from the northern Apennines (Italy), are detected in the studied stratigraphic interval (Fig. 9). The FO of *Reticulofenestra reticulata* (*Cribrocentrum reticulatum*) has been detected at 130 m. The FCO of *Dictyococcites scrippsae* (*D. hesslandii* of Backman, 1987) at 137 m seems to be a distinct event, although rare specimens are present from the base of the studied interval. This event could approximate the CP14b or zone NP17 (Lyle et al., 2002), which is marked by the LO of *Chiasmolithus solitus*. A major change in the nannofossil content is marked by the FCO of *Dictyococcites bisectus* >10 µm at around 145–148 m, which becomes abundant at 148–149 m (Fig. 9).

Oxygen and Carbon Isotopes

Bulk carbon isotope values (Fig. 10) range between +1.2‰ and +2.2‰, which correspond

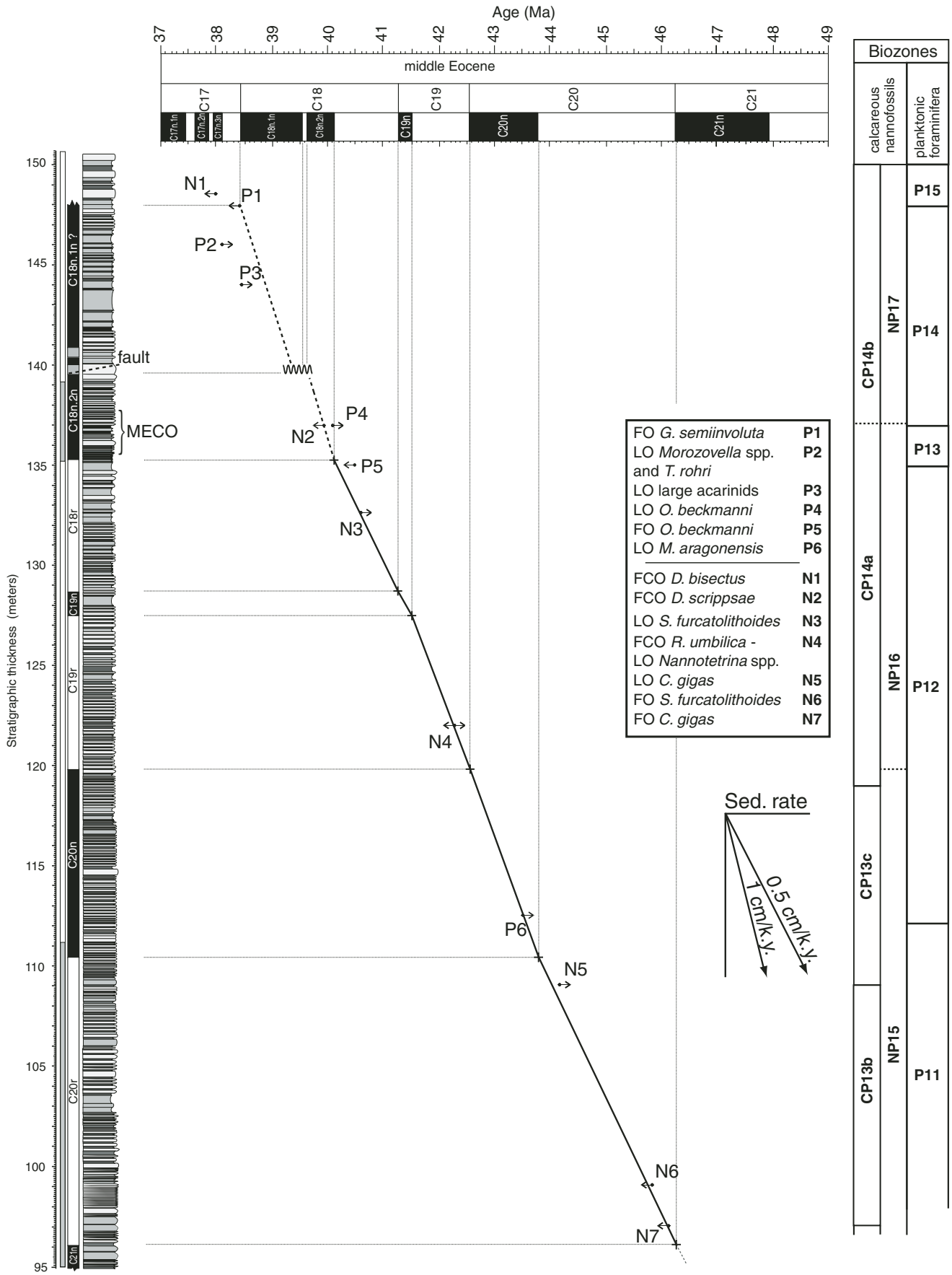
Age (Ma)
37
38
39
40
41
42
43
44
45
46
47
48
49
middle Eocene
C17
C18
C19
C20
C21
C17n.1n
C17n.2n
C17n.3n
C18n.1n
C18n.2n
C19n
C20n
C21n
Biozones
calcareous nannofossils
planktonic foraminifera
CP14b
CP14a
CP13c
CP13b
NP17
NP16
NP15
P15
P14
P13
P12
P11
Stratigraphic thickness (meters)
150
145
140
135
130
125
120
115
110
105
100
95
C18n.1n ?
C18n.2n
C18r
C19r
C19n
C20n
C20r
C21n
fault
MECO
N1
P1
P2
P3
P4
N2
P5
N3
N4
P6
N5
N6
N7
FO G. semiinvoluta P1
LO Morozovella spp. and T. rohri P2
LO large acarinids P3
LO O. beckmanni P4
FO O. beckmanni P5
LO M. aragonensis P6
FCO D. bisectus N1
FCO D. scrippsae N2
LO S. furcatolithoides N3
FCO R. umbilica - LO Nannotetrina spp. N4
LO C. gigas N5
FO S. furcatolithoides N6
FO C. gigas N7
Sed. rate
0.5 cm/k.y.
1 cm/k.y.

Figure 9. Age versus stratigraphic thickness plot with correlation of the Contessa Highway section polarity zonation to the geomagnetic polarity time scale (GPTS). Calcareous nannofossil (N) and planktonic foraminiferal (P) datums are used to constrain the interpretation. Planktonic foraminiferal zones are after Berggren et al. (1995); calcareous nannofossil zones are after (NP) Martini (1971) and (CP) Okada and Bukry (1980). MECO—middle Eocene climatic optimum; FO—first occurrence; FCO—first common occurrence; LO—last occurrence.

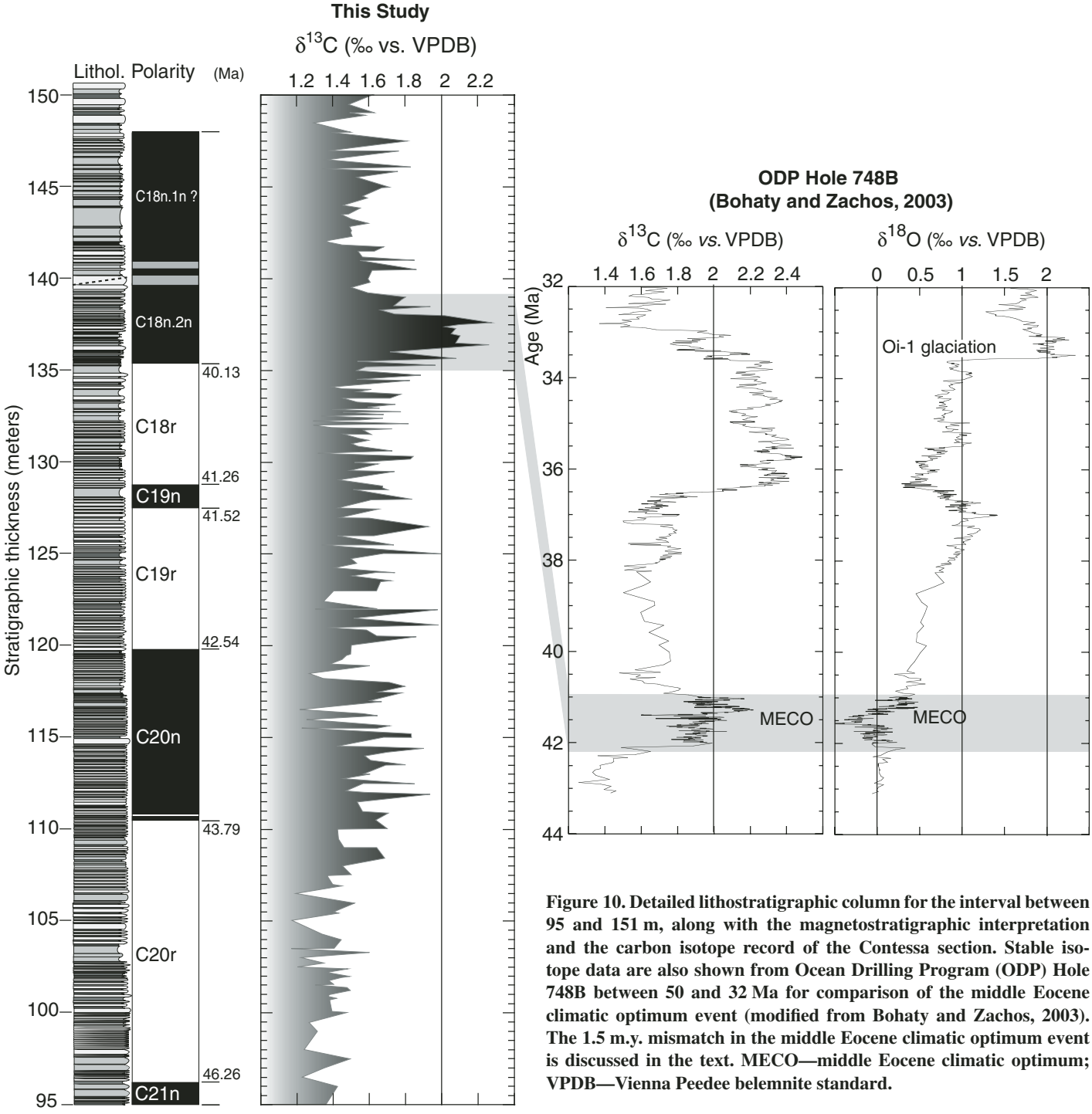

Figure 10. Detailed lithostratigraphic column for the interval between 95 and 151 m, along with the magnetostratigraphic interpretation and the carbon isotope record of the Contessa section. Stable isotope data are also shown from Ocean Drilling Program (ODP) Hole 748B between 50 and 32 Ma for comparison of the middle Eocene climatic optimum event (modified from Bohaty and Zachos, 2003). The 1.5 m.y. mismatch in the middle Eocene climatic optimum event is discussed in the text. MECO—middle Eocene climatic optimum; VPDB—Vienna Peedee belemnite standard.

to values for biogenic calcite precipitated under open-marine conditions during the Paleocene and Eocene (e.g., Bohaty and Zachos, 2003). On the other hand, $\delta^{18}O$ values (not shown here) range between –3.5‰ and –0.5‰ and are depleted by ~3‰ relative to diagenetically unaltered marine calcite (Bohaty and Zachos, 2003). We interpret these data to suggest that the oxygen isotopic composition of the measured samples reflects elevated temperature during burial diagenesis and/or the effects of meteoric diagenesis, while the carbon isotopic composition has been less affected by these processes. It is noteworthy that a global significance of the $\delta^{13}C$ signal has been previously inferred in other stratigraphic intervals of the Paleogene in the Contessa Highway section (e.g., Corfield et al., 1991).

The $\delta^{13}C$ curve contains a long positive excursion that rises from average values of 1.4‰ at the base of the studied section to a maximum of almost 2‰ at 112 m. Higher-frequency oscillations of ±0.3‰ about an average $\delta^{13}C$ value of 1.6‰ characterize the signal above the positive excursion at 112 m. The most notable feature of the $\delta^{13}C$ curve is a positive peak that rises by 0.6‰, starting at 133.5 m and peaking at ~138.5 m. After the peak, the $\delta^{13}C$ values swing back to average values of ~1.6‰ between 138.5 and 139.5 m.

DISCUSSION

Correlation to the Geomagnetic Polarity Time Scale

We provide here an interpretation of the magnetic polarity pattern of the middle Eocene Scaglia limestones that crop out in the Contessa Highway section, constrained by new analyses of planktic foraminifera and calcareous nannofossil assemblages. The geomagnetic polarity time scale (GPTS) used in this study is that of Berggren et al. (1995) and Cande and Kent (1995). Our magnetostratigraphic interpretation for the interval between 95 and 139 m is straightforward and provides a direct correlation with the GPTS between the top of chron C21n (46.26 Ma) and chron C18n.2n (39.63–40.13 Ma) (Fig. 9). Most of the recorded bioevents fall on or near the correlation line between our magnetic polarity zonation and the GPTS. Of these events, the LO of *Morozovella* spp. and *Truncorotaloides rohri* (P2) do not fall on the magnetostratigraphic correlation line, which might be related to the presence of the fault zone between 139.5 and 140 m. Above 140 m, the FCO of *Dictyococcites bisectus* (N1) and the FO of *Globigerinatheka semiinvoluta* (P1) suggest the possibility that the uppermost portion of magnetozone N4 above the fault zone correlates to chron C18n.1n. With this interpretation, at minimum, subchron C18n.1r (39.55–39.63 Ma) is inferred to be missing in the fault zone between 139.5 and 140 m. The average sedimentation rate for the interval between 135.29 m (base of chron C18n.2n) and 96.08 m (top of chron C21n) is 6.4 m/m.y. (0.64 cm/k.y.). Previous estimates of the sedimentation rate in the Eocene Scaglia Variegata and Scaglia Rossa Formations, as deduced from paleontological dating and the numerical time scale of Hardenbol and Berggren (1978), were of the order of 9 m/m.y. (see Lowrie et al., 1982).

Stable Isotopes and the Middle Eocene Climatic Optimum Event

On the basis of the correlation to the GPTS, the distinct ~0.6‰ increase in bulk $\delta^{13}C$ values observed in the middle Eocene of the Contessa Highway section occurred from the top of chron C18r through to subchron C18n.2n at ca. 40 Ma (Figs. 9 and 10). The magnitude and duration of the $\delta^{13}C$ shift are comparable to the middle Eocene climatic optimum stable isotope anomaly (positive shift of ~0.6‰ and duration of ~600 k.y.), which has been observed in multiple records from the Indian-Atlantic sector of the Southern Ocean and is interpreted as an interval of "significant transient warming" (Bohaty and Zachos, 2003). In these records, the age of the middle Eocene climatic optimum event was calculated primarily from calcareous nannofossil datums and was placed at 41.5 Ma. At Maud Rise (Ocean Drilling Program [ODP] Sites 689) and Kerguelen Plateau (ODP sites 738 and 748), the event is associated with the FO of the nannofossil *Reticulofenestra reticulata (*ex *Cribrocentrum reticulatum*), which occurs just below the middle Eocene climatic optimum event. The 1.5 m.y. mismatch between the middle Eocene climatic optimum event identified in Southern Ocean deep-sea cores and the stable isotope anomaly identified at the Contessa Highway section might reflect the uncertain calibration of *R. reticulata* in Southern Ocean sections. Crucially, the Kerguelen Plateau ODP sites do not have a reliable magnetostratigraphy in the vicinity of the middle Eocene climatic optimum event. The original magnetostratigraphic studies of these sites are unreliable, and a recent reanalysis demonstrated that this interval in ODP Hole 748B was weakly and unstably magnetized (Roberts et al., 2003).

Among the Southern Ocean records, ODP Hole 690B probably has the best middle Eocene magnetostratigraphic record, but this part of the section is riddled with hiatuses (Florindo and Roberts, 2005). There, the FO of *R. reticulata* occurs just below a normal polarity interval (see Figures 12 and 13 of Florindo and Roberts, 2005), which was interpreted to correlate with chron C19n, although it is also possible that this polarity interval could represent the bottom of C18n.2n.

In Hole 1090B (ODP Leg 177), the FO of *R. reticulata* occurs near the C18r/C19n reversal (Marino and Flores, 2002). The quality of the inclination data below ~C17n (~345 m below seafloor [mbsf]), however, is not good, so this might not be the best site from which to calibrate this datum. In Hole 1172A (ODP Leg 189), the FO of *R. reticulata* occurs between 414.29 and 417.29 mbsf (Wei et al., 2003), just below the base of C18n.2n at 415 mbsf (Stickley et al., 2004). However, it is worth noting that nannofossils are sparse below ~415 mbsf and this may not therefore represent the "true" FO of *R. reticulata*. Overall, the Southern Ocean data indicate that the age of the middle Eocene climatic optimum event remains poorly calibrated.

CONCLUSIONS

New magnetobiostratigraphic results from the middle Eocene Scaglia limestones of the Contessa Highway section can be directly correlated to the GPTS from chron C21n through to subchron C18n.1n, corresponding to the time interval between ca. 46.5 and 38.5 Ma (Berggren et al., 1995). A significant fault zone occurs in the upper part of the Contessa Highway section, which has removed, in our interpretation, at least subchron C18n.1r.

Bulk carbon isotope values indicate a distinct increase in bulk $\delta^{13}C$ values at the top of chron C18r through to subchron C18n.2n at ca. 40 Ma. This carbon shift is comparable in magnitude and duration to the middle Eocene climatic optimum stable isotope anomaly recently observed in multiple records from the Indian-Atlantic sector of the Southern Ocean dated at ca. 41.5 Ma (Bohaty and Zachos, 2003). It is noteworthy that just following the observed stable isotope anomaly (i.e., the middle Eocene climatic optimum event), a significant biotic turnover in planktonic foraminifera took place with a notable reduction in the acarinid lineage and the extinction of the morozovellids and other muricate species. This might suggest connected causal mechanisms between these events.

Our data from the Contessa Highway section provide the first evidence of the middle Eocene climatic optimum event beyond the Southern Ocean, which suggests a global response of the oceanic carbon cycle to the same forcing and that this forcing was not confined to the Indian and Atlantic sector of the Southern Ocean. We suggest that the ~1.5 m.y. mismatch might reflect significant uncertainty in the calibration of *R. reticulata* in Southern Ocean sedimentary sequences. Finally, high-frequency rhythms were

recognized in our new bed-by-bed lithological profile of the Scaglia Variegata Formation (with variable bundling of marly limestone–marl couplets). The next step is to conduct a detailed investigation to determine whether these cycles were orbitally controlled.

ACKNOWLEDGMENTS

The biostratigraphic study was carried out within the framework of the "Paleogene Integrated Stratigraphy" (PALIS) project established and sponsored by the Centro di Geobiologia of the University of Urbino. We are grateful to Cristano Collettini for his help on earlier versions of Figure 1 and to Michael Winklhofer for providing software for plotting FORC diagrams. We appreciate the insightful review comments by William Lowrie and Associate Editor Don McNeill.

REFERENCES CITED

Backman, J., 1987, Quantitative calcareous nannofossil biochronology of middle Eocene through early Oligocene sediments from DSDP Site 522 and 523: Abhandlungen der Geologische Bundesanstalt, v. 39, p. 21–31.

Berggren, W.A., Kent, D.V., Swisher, C.C., III, and Aubry, M.-P., 1995, A revised Cenozoic geochronology and chronostratigraphy, *in* Berggren, W.A., Kent, D.V., Aubry, M.P., and Hardenbol, J., eds., Geochronology, Time Scales and Global Stratigraphic Correlation: A Unified Temporal Framework for a Historical Geology: Society of Economic Paleontologists and Mineralogists (SEPM) Special Publication 54, p. 129–212.

Blow, W.H., 1969, Late middle Eocene to Recent planktonic foraminiferal biostratigraphy, *in* Brönniman, P., and Renz, H.H., eds., Proceedings of the 1st International Conference on Planktonic Microfossils (Geneva, 1967): Leiden, E.J. Brill, v. 1, p. 199–421.

Blow, W.H., 1979, The Cenozoic Globigerinida: A Study of the Morphology, Taxonomy, Evolutionary Relationships and the Stratigraphical Distribution of some Globigerinida (mainly Globigerinacea): Leiden, E.J. Brill, v. 3, p. 1413.

Bohaty, S.M., and Zachos, J.C., 2003, Significant Southern Ocean warming event in the late middle Eocene: Geology, v. 31, p. 1017–1020, doi: 10.1130/G19800.1.

Bolli, H.M., 1957a, The genera *Globigerina* and *Globorotalia* in the Paleocene–Lower Eocene Lizard Springs Formation of Trinidad: B.W.I: U.S. National Museum Bulletin, v. 215, p. 51–81.

Bolli, H.M., 1957b, Planktonic foraminifera from the Eocene Navet and San Fernando Formations of Trinidad: B.W.I: U.S. National Museum Bulletin, v. 215, p. 155–172.

Bolli, H.M., 1966, Zonation of Cretaceous to Pliocene marine sediments based on planktonic foraminifera: Boletino Informativo Associacion Venezolana de Geologia, Mineria y Petrolio, v. 9, p. 3–32.

Bown, P.R., and Young, J., 1998, Techniques, *in* Bown, P.R., ed., Calcareous Nannofossil Biostratigraphy: London, Chapman & Hall, p. 16–28.

Cande, S.C., and Kent, D.V., 1995, Revised calibration of the geomagnetic polarity time scale for the late Cretaceous and Cenozoic: Journal of Geophysical Research, v. 100, p. 6093–6095, doi: 10.1029/94JB03098.

Catanzariti, R., and Perilli, N., 2004, Nannobiohorizons recognised in Eocene Formations from the northern Apennines (Italy): Ina10 Abstracts, Lisbon: Journal of Nannoplankton Research, v. 26, p. 16–17.

Channell, J.E.T., D'Argenio, B., and Horwath, F., 1979, Adria, the African Promontory, *in* Mesozoic Mediterranean Palaeogeography: Earth-Science Review, v. 15, p. 213–292.

Corfield, R.M., Cartlidge, J.E., Premoli-Silva, I., and Housley, R.A., 1991, Oxygen and carbon isotope stratigraphy of the Palaeogene and Cretaceous limestones in the Bottaccione Gorge and the Contessa Highway sections, Umbria, Italy: Terra Nova, v. 3, p. 414–422.

Cresta, S., Monechi, S., and Parisi, G., 1989, Stratigrafia del Mesozoico al Cenozoico nell'area Umbro-Marchigiana: Memorie Descrittive della Carta Geologica d'Italia, v. 34, p. 185.

Florindo, F., and Roberts, A.P., 2005, Eocene-Oligocene magnetobiochronology of ODP Sites 689 and 690, Maud Rise, Weddell Sea, Antarctica: Geological Society of America Bulletin, v. 117, p. 46–66, doi: 10.1130/B25541.1.

Goree, W.S., and Fuller, M., 1976, Magnetometers using RF-driven squids and their applications in rock magnetism and paleomagnetism: Reviews of Geophysics and Space Physics, v. 1, p. 591–608.

Guerrera, F., Monaco, P., Nocchi, M., Parisi, G., Franchi, R., Vannucci, S., and Giovannini, G., 1988, La Scaglia Variegata Eocenica nella sezione di Monte Cagnero (bacino marchigiano interno): Studio litostratigrafico, petrografico e biostratigrafico: Bollettino Società Geologica Italiana, v. 107, p. 81–99.

Hardenbol, J., and Berggren, W.A., 1978, A new Paleogene numerical time scale, *in* Cohee, G.V., Glaessner, M.F., and Hedberg, H.D., eds., Contributions to the Geologic Time Scale; Studies in Geology: Tulsa, Oklahoma, American Association of Petroleum Geologists, v. 6, p. 213–234.

Kirschvink, J.L., 1980, The least-squares line and plane and the analysis of palaeomagnetic data: Geophysical Journal of the Royal Astronomical Society, v. 62, p. 699–718.

LaBrecque, J.L., Kent, D.V., and Cande, S.C., 1977, Revised magnetic polarity time scale for Late Cretaceous and Cenozoic time: Geology, v. 5, p. 330–335, doi: 10.1130/0091-7613(1977)5<330:RMPTSF>2.0.CO;2.

Lear, C.H., Rosenthal, Y., Coxall, H.K., and Wilson, P.A., 2004, Late Eocene to early Miocene ice sheet dynamics and the global carbon cycle: Paleoceanography, v. 19, PA4015, doi: 10.1029/2004PA001039.

Lirer, F., 2000, A new technique for retrieving calcareous microfossils from lithified lime deposits: Micropaleontology, v. 46, p. 365–369.

Lowrie, W., Alvarez, W., Napoleone, G., Perch-Nielsen, K., Premoli Silva, I., and Toumarkine, M., 1982, Paleogene magnetic stratigraphy in Umbrian pelagic carbonate rocks: The Contessa sections, Gubbio: Geological Society of America Bulletin, v. 93, p. 414–432, doi: 10.1130/0016-7606(1982)93<414:PMSIUP>2.0.CO;2.

Lyle, M., Wilson, P.A., Janecek, T.R., et al., 2002, Proceedings of the Ocean Drilling Program Initial reports, Volume 199: College Station, Texas, Ocean Drilling Program, http://www-odp.tamu.edu/publications/199_IR/199ir.htm.

Marino, M., and Flores, J.A., 2002, Middle Eocene to early Oligocene calcareous nannofossil stratigraphy at Leg 177 Site 1090: Marine Micropaleontology, v. 45, p. 383–398, doi: 10.1016/S0377-8398(02)00036-1.

Martini, E., 1971, Standard Tertiary and Quaternary calcareous nannoplankton zonation, *in* Farinacci, A., eds., Proceedings of the Second Planktonic Conference, Rome 1970: Rome, Tecnoscienza, v. 2, p. 739–785.

Mattias, P., Farabollini, P., and Montanari, A., 1989, Aspetti minero-petrografici della Scaglia Variegata nella serie pelagica della valle della Contessa, presso Gubbio, Umbria orientale: Studi Geologici Camerti, v. 11, p. 7–14.

Miller, K.G., Wright, J.D., and Fairbanks, R.G., 1991, Unlocking the ice house: Oligocene-Miocene oxygen isotopes, eustasy and margin erosion: Journal of Geophysical Research, v. 96, p. 6829–6848.

Monaco, P., Nocchi, M., and Parisi, G., 1987, Analisi stratigrafica e sedimentologica di alcune sequenze pelagiche dell'Umbria sud-orientale dall'Eocene inferiore all'Oligocene inferiore: Bollettino Società Geologica Italiana, v. 106, p. 71–91.

Monechi, S., and Thierstein, H.R., 1985, Late Cretaceous–Eocene nannofossil and magnetostratigraphic correlations near Gubbio, Italy: Marine Micropaleontology, v. 9, p. 419–440, doi: 10.1016/0377-8398(85)90009-X.

Montanari, A., Bice, D.M., Capo, R., Coccioni, R., Deino, A., De Paolo, D.J., Emmanuel, L., Monechi, S., Renard, M., and Zevenboom, D., 1997, Integrated stratigraphy of the Chattian to mid-Burdigalian pelagic sequence of the Contessa valley (Gubbio, Italy), *in* Montanari, A., Odin, G.S., and Coccioni, R., eds., Miocene Stratigraphy: An Integrated Approach: Amsterdam, Elsevier Sciences, p. 249–277.

Okada, H., and Bukry, D., 1980, Supplementary modification and introduction of code numbers to the low-latitude coccolith biostratigraphic zonation (Bukry, 1973, 1975): Marine Micropaleontology, v. 5, p. 321–325, doi: 10.1016/0377-8398(80)90016-X.

Pearson, P.N., and Chaisson, W.P., 1997, Late Paleocene to middle Miocene planktonic foraminifer biostratigraphy, *in* Miller, C.M., and Riegel, R.N., et al., Proceedings of the Ocean Drilling Program, Scientific results, Volume 154: College Station, Texas, Ocean Drilling Program, p. 33–68.

Perch-Nielsen, K., 1985, Mesozoic calcareous nannofossils, *in* Bolli, H.M., Saunders, J.B., and Perch-Nielsen, K., eds., Plankton Stratigraphy: Cambridge, Cambridge University Press, p. 329–426.

Premoli Silva, I., and Bolli, H.M., 1973, Late Cretaceous to Eocene planktonic foraminifera and stratigraphy of Leg 15 sites in the Caribbean Sea, *in* Edgar, N.T., Saunders, J.B. et al., Initial Reports of the Deep Sea Drilling Project, Volume 15: Washington, D.C., Government Printing Office, p. 449–547.

Premoli Silva, I., Rettori, R., and Verga, D., 2003, Practical Manual of Paleocene and Eocene Planktonic Foraminifera: Perugia (Italy), Tipografia Pontefelcino, 152 p.

Roberts, A.P., Pike, C.R., and Verosub, K.L., 2000, FORC diagrams: A new tool for characterizing the magnetic properties of natural samples: Journal of Geophysical Research, v. 105, p. 28,461–28,475, doi: 10.1029/2000JB900326.

Roberts, A.P., Bicknell, S.J., Byatt, J., Bohaty, S.M., Florindo, F., and Harwood, D.M., 2003, Magnetostratigraphic calibration of Southern Ocean diatom datums from the Eocene–Oligocene of Kerguelen Plateau (Ocean Drilling Program Sites 744 and 748): Palaeogeography, Palaeoclimatology, Palaeoecology, v. 198, p. 145–168, doi: 10.1016/S0031-0182(03)00397-3.

Shackleton, N.J., and Kennett, J.P., 1975, Paleotemperature history of the Cenozoic and the initiation of Antarctic glaciation: Oxygen and carbon isotope analyses in DSDP Sites 277, 279, and 281: Initial Reports of the Deep Sea Drilling Project, Volume 29: Washington, D.C., Government Printing Office, p. 743–755.

Spötl, C., and Vennemann, T.W., 2003, Continuous-flow isotope ratio mass spectrometric analysis of carbonate minerals: Rapid Communications in Mass Spectrometry, v. 17, p. 1004–1006, doi: 10.1002/rcm.1010.

Stacey, F.D., and Banerjee, S.K., 1974, The Physical Principles of Rock Magnetism: New York, Elsevier, 195 p.

Stickley, C.E., Brinkhuis, H., McGonigal, K.L., Chaproniere, G.C.H., Fuller, M., Kelly, D.C., Nürnberg, D., Pfuhl, H.A., Schellenberg, S.A., Schoenfeld, J., Suzuki, N., Touchard, Y., Wei, W., Williams, G.L., Lara, J., and Stant, S.A., 2004, Late Cretaceous–Quaternary biomagnetostratigraphy of ODP Sites 1168, 1170, 1171, and 1172, Tasmanian Gateway, *in* Exon, N.F., Kennett, J.P., and Malone, M.J., et al., Proceedings of the Ocean Drilling Program, Scientific results, Volume 189: http://www-odp.tamu.edu/publications/189_SR/111/111.htm (August 2004).

Van Morkhoven, F.P.C.M., Berggren, W.A., and Edwards, A.S., 1986, Cenozoic cosmopolitan deep-water benthic foraminifera: Bulletin des Centres Recherche Exploration—Production Elf-Aquitane Memoir 11, 421 p.

Varol, O., 1998, Paleogene, *in* Bown, P.R., ed., Calcareous Nannofossil Biostratigraphy: Dordrecht, Kluwer Academic Publishing, p. 201–224.

Verducci, M., and Nocchi, M., 2004, Middle to late Eocene main planktonic foraminiferal events in the Central Mediterranean area (Umbria-Marche basin) related to paleoclimatic changes: Neues Jahrbuch für Geologie und Paläontologie Abhandlungen, v. 234, p. 361–413.

Wei, W., McGonigal, K.L., and Zhong, S., 2003, Data report: Paleogene calcareous nannofossil biostratigraphy of ODP Leg 189 (Australia-Antarctica Gateway), *in* Exon, N.F., Kennett, J.P., Malone, M.J., et al., Proceedings of the Ocean Drilling Program, Scientific results, Volume 189: http://www-odp.tamu.edu/publications/189_SR/103/103.htm (July 2003).

Zachos, J.C., Pagani, M., Sloan, L., Thomas, E., and Billups, K., 2001, Trends, rhythms, and aberrations in global climate 65 Ma to present: Science, v. 292, p. 686–693, doi: 10.1126/science.1059412.

Zijderveld, J.D.A., 1967, AC demagnetization of rocks: Analysis of results, *in* Collinson, D.W., ed., Methods in Paleomagnetism: New York, Elsevier Sciences, p. 254–286.

Manuscript Received 18 October 2005
Revised Manuscript Received 30 October 2006
Manuscript Accepted 28 November 2006

Printed in the USA